Solar Energy Materials & Solar Cells 158 (2016) 130–137

Contents lists available at ScienceDirect

Solar Energy Materials & Solar Cells

journal homepage: www.elsevier.com/locate/solmat

Selenization kinetics in $Cu_2ZnSn(S,Se)_4$ solar cells prepared from nanoparticle inks

Yongtao Qu, Guillaume Zoppi, Neil S. Beattie *

Department of Physics and Electrical Engineering, Ellison Building, Northumbria University, Newcastle upon Tyne NE1 8ST, UK

ARTICLE INFO

Article history:
Received 24 July 2015
Received in revised form
3 November 2015
Accepted 3 December 2015
Available online 28 December 2015

Keywords:
CZTS
Nanoparticle inks
CZTSSe
Selenization
Solar cell

ABSTRACT

Earth-abundant $Cu_2ZnSn(S,Se)_4$ (CZTSSe) thin film photovoltaic absorber layers are fabricated by annealing Cu_2ZnSnS_4 (CZTS) nanoparticle thin films in a selenium rich atmosphere. Systematic variation of the selenization time (5, 10, 20 and 40 min) and temperature (450, 500, 550 and 600 °C) provides insight into the kinetics of the selenization process and in particular recrystallization and grain growth. Se–S anion exchange is found to follow Avrami's model in which the CZTS selenization is controlled by an irregular one-dimensional process limited by metal cation re-ordering and grain boundary migration. CZTSSe grain growth is observed to follow a normal relation with a grain growth exponent close to the ideal case of equiaxed grains and the grain boundary migration energy is calculated to be 85.38 kJ/mol. These selenization variables have a fundamental influence on the quality of the resulting CZTSSe thin film and consequently the device performance. A peak device solar energy conversion efficiency of 5.4% was obtained for selenization at 500 °C for 20 min. The device efficiency was found to be highly sensitive to these variables and it is critical to obtain an appropriate balance between grain growth and thin film quality.

1. Introduction

With the advantage of outstanding optoelectronic properties and earth-abundant constituents, $Cu_2ZnSn(S,Se)_4$ (CZTSSe) is a promising alternative thin film photovoltaic (PV) material experiencing rapid progress in recent years [1–6]. CZTSSe technology is expected to benefit from the rich research experience of Cu(In,Ga)Se_2 (CIGS) because of the material similarities. Among the variety of techniques employed for preparation of the absorber films, the best results are observed for a hydrazine solution based method with efficiency up to 12.6% [7]. On the other hand, Cu_2ZnSnS_4 (CZTS) nanoparticle inks and subsequent selenization offers a non-toxic route to fabricate high quality PV absorber layers and can yield cell efficiencies as high as 9.0% [8]. We have previously shown that by tuning the chemical reaction conditions, CZTS nanoparticle properties such as crystal structure and bandgap energy can be controlled and that the performance of thin film solar cells fabricated using this technique depends critically on the nanoparticle inks [9,10].

In addition to the nanoparticle ink, a key step in the fabrication of high quality CZTSSe thin film PV absorber layers is high temperature selenization. Here the goal is to convert CZTS nanoparticles into large CZTSSe grains while minimizing the number of grain boundaries. Despite the importance of this step to the production of efficient CZTSSe thin film solar cells, the film morphology and composition variations that occur during the selenization process lacks in-depth investigation. In most cases, only selected selenization conditions are reported to yield absorber layers suitable for subsequent device fabrication [11,12]. In order to optimize this part of the fabrication process it is important to understand the grain growth kinetics and in this work we report experiments in which the selenization conditions are systematically controlled. The results indicate that the PV absorber layer morphology and composition are strongly influenced by the selenization conditions and play important roles in determining the performance of solar cells made from these absorbers.

2. Experimental procedure

CZTS nanoparticles used in the study were produced by injection of metallic precursors into a hot surfactant. The resulting nanoparticle inks were deposited on molybdenum substrates via spin coating. This process has been described in greater detail in our previous works [9,10].

* Corresponding author.
E-mail address: neil.beattie@northumbria.ac.uk (N.S. Beattie).

http://dx.doi.org/10.1016/j.solmat.2015.12.016

2.1. Selenization of CZTS precursor films

To induce grain growth, CZTS nanoparticle thin films were selenized in a tube furnace. The as-deposited precursor thin films were 1 μm thick and were placed inside a cylindrical graphite box with selenium pellets placed directly beneath the substrate. The furnace was evacuated (6.0×10^{-3} mbar) and backfilled with argon (~10 mbar) prior to increasing the temperature (~20 °C/min) from room temperature to the selenization temperature where it was held constant for a given time. Two series of experiments were conducted to systematically study dynamic variations of the morphology and composition during the selenization process. Time-dependent experiments were performed by setting the selenization time to 5, 10, 20 and 40 min with the temperature held at 500 °C. Temperature-dependent experiments were performed by setting the temperature to 450, 500, 550 and 600 °C for a period of 20 min. All time and temperature dependent experiments were performed with ~300 mg of selenium loaded in the graphite box. After selenization, the tube furnace was cooled rapidly to 300 °C using a fan in just 10 min. This was followed by slower cooling to 50 °C in a further 60 min. As the graphite box was only partially closed, the selenium partial pressure inside the graphite box was not constant during the initial temperature ramp. Upon heating, the selenium evaporates and escapes into quartz tube until equilibrium is reached, where the temperature is stable at the given selenization temperature. The equilibrium selenium vapor pressure can be estimated using the model developed by Scragg [13]. In this work the partial pressure of selenium P_{e,Se_2} within the graphite box after pressure equilibration was stable at 0.13 bar for time-dependent experiments. For the temperature-dependent measurements, P_{e,Se_2} increased only slightly from 0.12 bar at 450 °C to 0.15 bar at 600 °C and its influence on the grain growth could be ignored.

2.2. Device fabrication

The resulting CZTSSe thin films were integrated in solar cell devices with the configuration: Mo/CZTSSe/CdS/i-ZnO/ITO/Ni–Al, where "i" stands for intrinsic and ITO is indium tin oxide. The CdS buffer layer was deposited using a chemical bath process. Deionized water was first poured into a double-walled beaker and after the temperature inside the reaction vessel stabilized at 70 °C, $CdSO_4$ (2 mM) and ammonium (1.5 M) were added successively. The CZTSSe films were then soaked in the solution for 2 min before thiourea (12 mM) was added. After the reaction, the samples were removed from the bath, rinsed with deionized water, dried under a nitrogen stream and then annealed at 200 °C for 10 min in air. The transparent oxide layers were deposited by magnetron sputtering using ~60 nm of i-ZnO and ~200 nm of ITO. Finally, the front contact grid was deposited by electron beam evaporation of Ni (~50 nm) and Al (~1 μm) through a shadow mask. Each solar cell was defined by mechanical scribing the substrate into nine 0.16 cm^2 devices.

2.3. Characterization

The film morphology and composition were determined using a FEI Quanta 200 scanning electron microscope (SEM) equipped with an Oxford Instruments energy dispersive X-ray spectroscopy (EDS). K_α X-ray emission lines for Cu, Zn, S and L_α for Sn were used for quantification. Current density–voltage (J–V) measurements were performed in a four-point probe configuration using a Keithley 2400 series source meter. Samples were illuminated with an Abet Technologies Sun 2000 solar simulator with an air mass (AM) 1.5 spectrum set at 100 mW/cm^2.

3. Results and discussion

3.1. Selenization process kinetics

To optimize the selenization process, time-dependent experiments were firstly performed to understand kinetic variations of morphology and composition during grain growth. Annealing times were therefore increased from 5 min to 40 min with the temperature fixed at 500 °C and a selenium vapor pressure of 0.13 bar. The cross sectional SEM images of the thin films are shown in Fig. 1.

The cross-sectional SEM images in Fig. 1 reveal three layers. The top layer is composed of a large-grained CZTSSe layer on top of a residual fine-grained CZTSSe (middle) layer. The bottom layer is typical of Mo with a columnar grain structure. Furthermore, under selenium rich selenization conditions, a thin additional layer (see Fig. 5) of $Mo(S,Se)_2$ forms at the interface between the Mo and fine-grained CZTSSe layers [8,14]. From Fig. 1, it is clear that a longer selenization period results in a thicker large-grained layer and a thinner fine-grained layer. However, the rate of grain growth is not constant during the selenization process: grain growth is initially fast and then slows for longer selenization times.

The reaction kinetics of the selenization process have previously been explained using a parabolic model [15,16]. In this model, the selenization process can be considered to be a solid–gas reaction as depicted in Fig. 2(a) where a layer of CZTSSe nuclei is formed at the interface between the CZTS precursor layer and the Se_2 gas layer at the start of the reaction. As the reaction proceeds, more selenium diffuses into the CZTS layer to induce

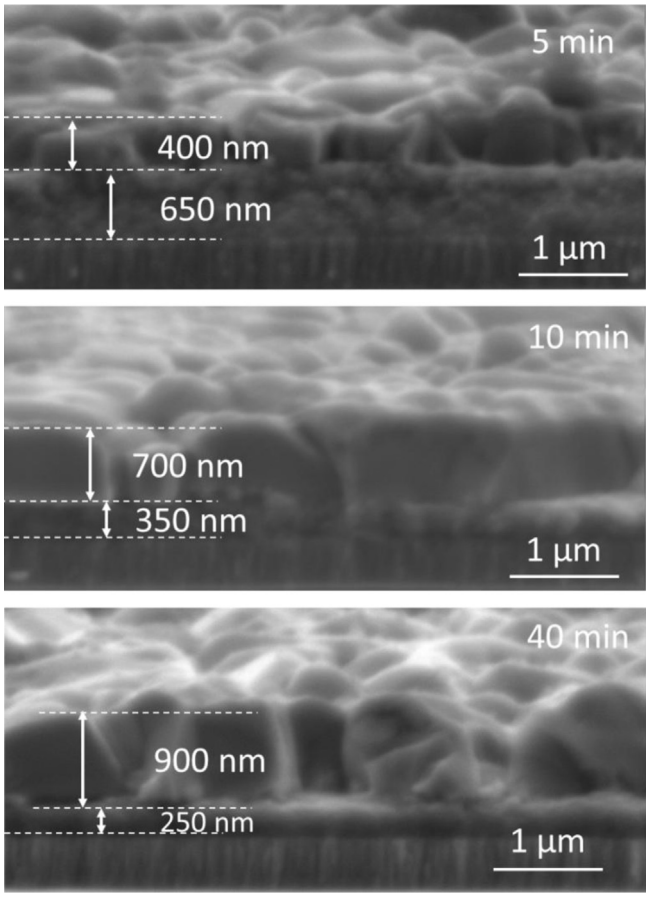

Fig. 1. Cross-sectional SEM images of CZTSSe thin films obtained at different selenization times each at 500 °C. From top to bottom, the three visible layers are the large-grained CZTSSe, small-grained CZTSSe and the Mo substrate.

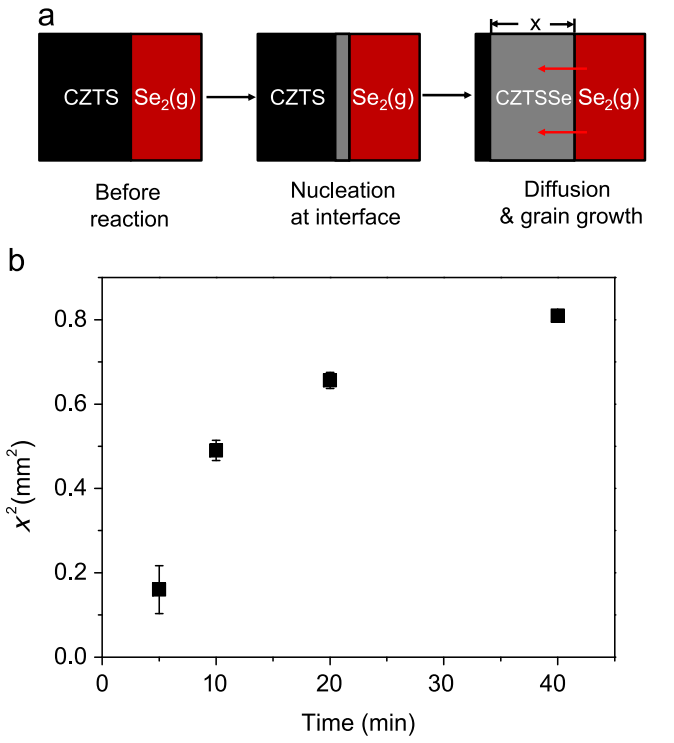

Fig. 2. (a) Schematic diagram of grain growth in a solid–gas reaction process. (b) Plot of large grain layer thickness squared versus heat treatment time.

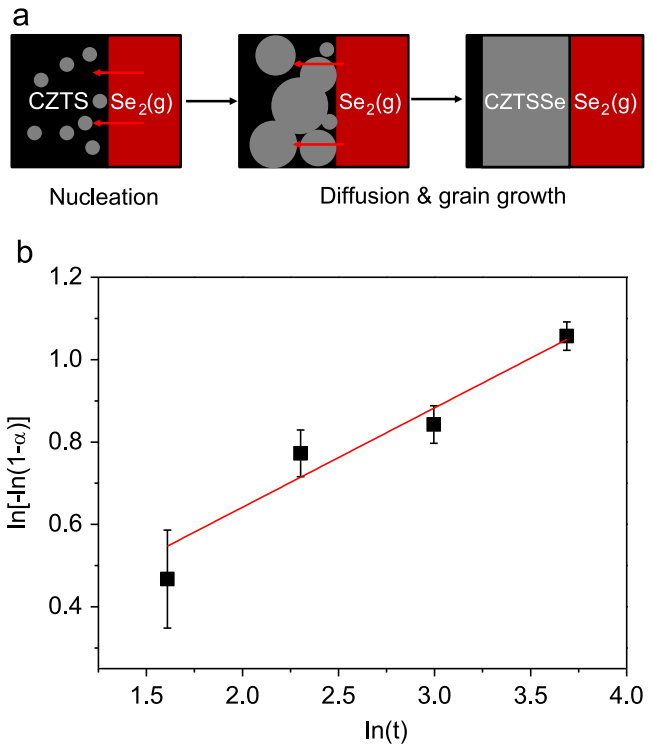

Fig. 3. (a) Schematic diagram of grain growth following Avrami's model. (b) Sharp–Hancock plot for CZTS selenized at 500 °C.

Table 1
Composition variations of sulfur and selenium in CZTSSe thin films for different selenization times at 500 °C.

Time (min)	S (at%)	Se (at%)	α=Se/(S+Se)
5	12.44	48.21	0.79
10	6.30	48.36	0.88
20	5.24	48.01	0.90
40	2.97	49.85	0.94

large-scale CZTSSe grain growth. The parabolic growth model is described by:

$$x^2(t) = K_p t + C \quad (1)$$

where $x(t)$ is the thickness (μm) of the CZTSSe layer, K_p is a rate constant (μm^2/min), t is heat treatment time (minutes) and C is a constant [17].

For parabolic grain growth, there should be a linear relationship between x^2 and t. However, as shown in Fig. 2(b), this is clearly not the case and suggests that the rate constant K_p, is time dependent. The parabolic model assumes that the diffusion of selenium anions is the rate-controlling step of the reaction and the diffusivity of the CZTSSe large grain layer is assumed to be a constant. This assumption implies that the resultant large grain should be uniform, continuous and of single phase during the heat treatment period. However, analysis of the thin films at different selenization times reveals that the composition of the absorber layer is time dependent. As shown in Table 1, about 80% of sulfur is replaced by selenium in the first 5 min of the heat treatment. This increases to 94% after 40 min. As a result, the CZTSSe grain growth reaction process cannot be simply described by the parabolic mode.

In addition to the parabolic model (solid–gas reaction process), CZTSSe grain growth reaction can be described as a phase transformation from parent CZTS phase to CZTSSe following Avrami's model [15,16]. This is illustrated in Fig. 3(a) where a significant number of CZTSSe nuclei are rapidly formed at the beginning of reaction under an isothermal process. As more selenium diffuses into the thin film during the intermediate period, nuclei grow into large grains by dissolution of the parent CZTS lattice and reformation of the selenium-based lattice. Once the conversion nears completion, there is little untransformed CZTS left for nuclei to form and the process begins to slow. The Avrami model is given as:

$$\ln[-\ln(1-\alpha)] = n_a \times \ln(K_a) + n_a \times \ln(t) \quad (2)$$

where α is conversion ratio and equals to Se/(S+Se), n_a is Avrami's exponent, K_a is Avrami's rate constant (min^{-1}) and t is heat treatment time (min). A plot of $\ln[-\ln(1-\alpha)]$ versus $\ln(t)$ (known as a Sharp–Hancock plot) is given in Fig. 3(b). Fitting Eq. (2) to these data yields an Avrami's exponent n_a and rate constant K_a of 0.24 and 1.95 min^{-1}, respectively. An Avrami exponent of <1 indicates that the selenization reaction is controlled by an irregular one-dimensional process limited by cation ordering and grain growth [16].

The half-selenization time $t_{\frac{1}{2}}$ can be calculated for α=0.5:

$$t_{\frac{1}{2}} = \frac{1}{K_a}(\ln 2)^{\frac{1}{n_a}} \quad (3)$$

Using the values of n_a and K_a obtained from Fig. 3, it only takes about 10 s to complete 50% of the selenium conversion. The relatively fast selenium incorporation therefore indicates that the CZTSSe grain growth is limited by cation re-ordering rather than selenium incorporation. This finding is consistent with the work reported by Mainz et al. that selenium incorporation is completed during the first few seconds of CIGS film formation [18]. However, longer annealing times are required for the formation of large grains.

CZTSSe grain growth process can be further studied by analyzing the grain sizes of the layer as this is an important parameter for the quality of polycrystalline thin films. Normal grain growth at a constant temperature can be explained by considering that the average grain radius r depends on the annealing time t through [19]:

$$r^n - r_o{}^n = Kt \quad (4)$$

where r is the average grain radius after selenziation (μm), r_0 is the initial grain radius (which here can be ignored as the initial nanoparticles are much smaller than the converted CZTSSe grains), K is the grain growth coefficient, n is the grain growth exponent and is expected to have a value of 2 when the as-deposited film has an equiaxed grain structure [19].

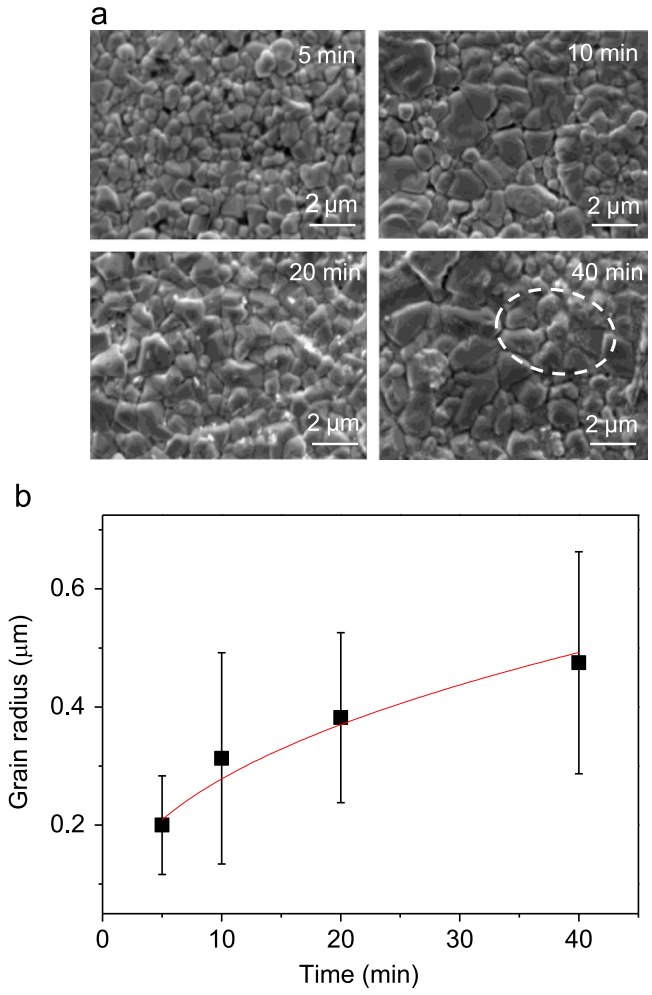

Fig. 4. (a) Top view SEM images and (b) the average grain radius of CZTSSe thin film for different selenization periods at 500 °C. The solid line is the fitted power function curve.

The average grain radius r of the CZTSSe thin film after annealing can be measured from top-view SEM images as shown in Fig. 4(a) where it is shown that longer selenization time results in larger grains. The average grain radius r determined from these data is plotted as a function of annealing period t in Fig. 4(b) and the value of the CZTSSe grain growth exponent n can be obtained by fitting a power function:

$$r \propto t^{0.41} \tag{5}$$

According to Eq. (4), this fitted curve yields $n=2.44$ which further indicates that the as-deposited thin film is formed by equiaxed grains. The grain growth coefficient is expressed as $K = K_o \exp\left(-\frac{Q}{RT}\right)$, and therefore the CZTSSe grain growth model can be revised into a temperature-dependent model:

$$\ln(r^{2.44}) = \ln(K_o t) - \frac{Q}{RT} \tag{6}$$

\where K_o is weakly temperature dependent and depends on grain geometry and average grain boundary energy, t is the selenization time, Q is the activation energy for grain boundary motion (kJ/mol), R is the gas constant (8.31 J mol^{-1} K^{-1}) and T is the selenization temperature (K). In order to test Eq. (6), a series of experiments were performed in which the selenization temperature was increased from 450 to 600 °C with a fixed dwell time of 20 min at each temperature. The top view and corresponding cross sectional SEM images of the thin films are shown in Fig. 5. As summarized in Fig. 6(a), the increased selenization temperature produces larger grains from less than 0.5 μm at 450 °C to more than 1.5 μm at 600 °C.

Furthermore, higher temperatures result in more selenium being incorporated into the lattice to facilitate grain growth (Table 2), which indicates that the selenium conversion process is both time and temperature dependent. Contrary to the selenium variation, the composition of metals in the thin films is relatively stable as the selenization temperature increases (with the exception of a slight loss of Sn at 600 °C) and unlikely to strongly influence the device performance. Similar to the time-dependent experiments, higher temperature results in thicker large-grained layers and thinner fine-grained layers (Fig. 5(e–h)). Once the thin films have an average grain size comparable to the thickness of the large-grained layer, the grain growth slows down and eventually stops resulting in columnar grain structures [19].

Based on Eq. (6), a plot of $\ln(r^{2.44})$ versus $\frac{1000}{T}$ is given in Fig. 6 (b). A linear fit indicates CZTSSe grain growth follows a normal grain growth process. From the slope of the fit, an energy of 85.38 kJ/mol is needed to activate the CZTSSe grain boundary migration to consume the small grains.

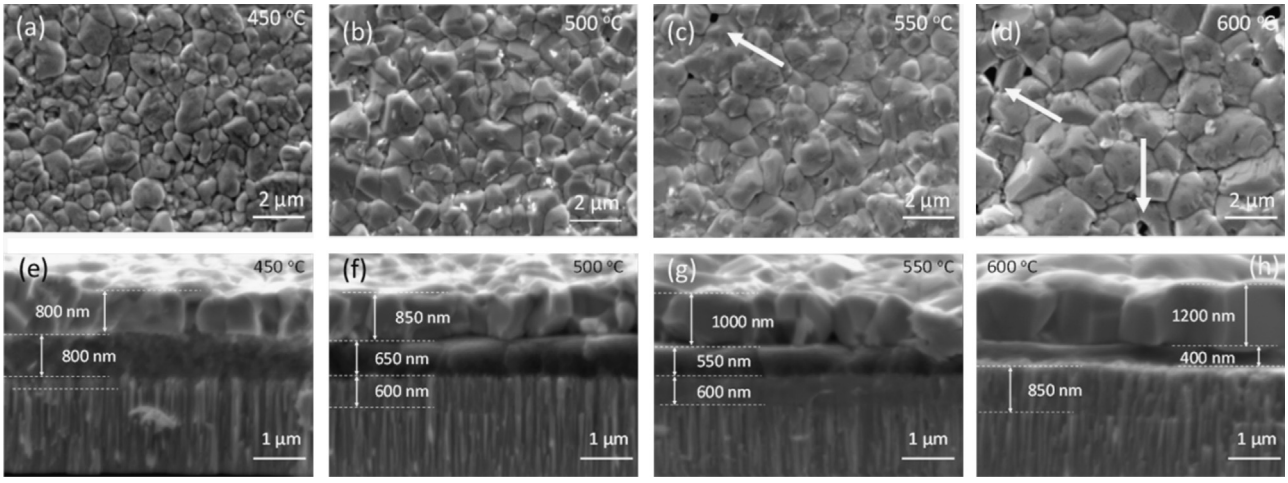

Fig. 5. Top-view (a–d) and cross sectional (e–h) SEM images of CZTSSe thin film obtained at different selenization temperatures for 20 min.

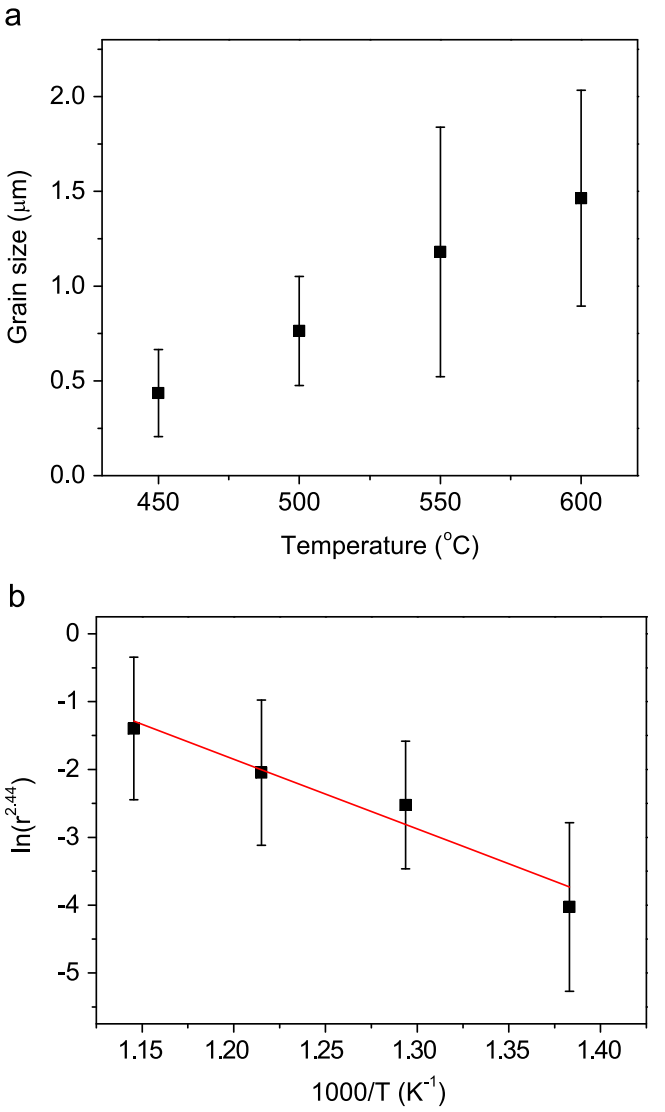

Fig. 6. (a) Average grain sizes at different temperature and (b) a plot of $\ln(r^{2.44})$ versus 1000/*T*.

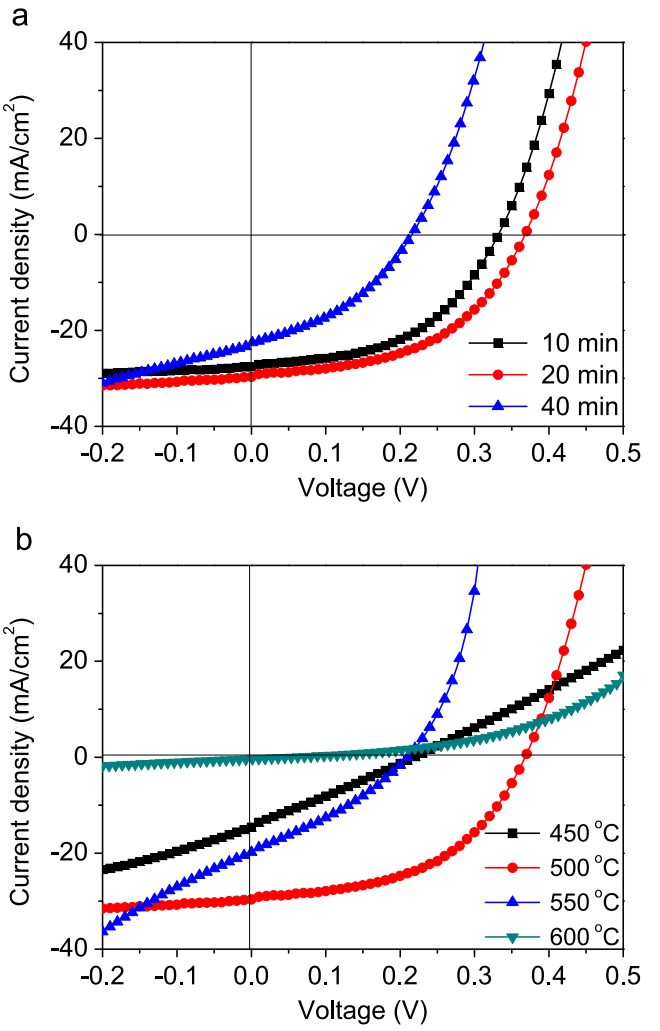

Fig. 7. (a) *J–V* curves of solar cells with CZTSSe thin film absorbers annealed for different times at 500 °C. (b) *J–V* curves of solar cells with CZTSSe thin film absorbers annealed at different temperatures for 20 min.

Table 2
Composition variations of sulfur and selenium in the thin films at different temperatures for a selenization time of 20 min.

Temp. (°C)	Zn/Sn	Cu/(Zn+Sn)	S (at%)	Se (at%)	α=Se/(S+Se)
450	1.06	0.89	8.51	45.24	0.84
500	1.07	0.90	5.24	48.01	0.90
550	1.06	0.87	4.47	50.05	0.92
600	1.16	0.86	3.89	51.07	0.93

3.2. Device performance

CZTSSe thin films prepared at different times and temperatures were embedded into solar cells and *J–V* curves obtained from the best devices at each selenization time are shown in Fig. 7(a) with the device parameters extracted from the *J–V* curves summarized in Table 3. Additionally, the distributions of solar energy conversion efficiency (η), open circuit voltage (V_{oc}), short circuit current density (J_{sc}), and fill factor (*FF*) from all nine devices on each substrate are shown in Fig. 8 demonstrating the high uniformity of device performance across the substrates.

Table 3
Device parameters for the solar cells with *J–V* curves shown in Fig. 7(a).

Device (min)	η (%)	V_{oc} (V)	J_{sc} (mA/cm^2)	*FF* (%)	R_S (Ω cm^2)	R_{SH} (Ω cm^2)
10	4.48	0.33	27.5	49.3	3.2	122
20	5.41	0.36	29.6	50.7	3.1	77
40	1.90	0.21	22.5	39.8	3.9	21

The device with an absorber layer selenized for 20 min exhibits the highest overall efficiency of η=5.41%, with V_{oc}=0.36 V, J_{sc}=29.6 mA/cm^2, and *FF*=50.7%. In distinct contrast, the efficiency of the device with an absorber that was selenized for 40 min is only η=1.90%. As shown in Table 3, the reduced efficiency of this device arises not only from reductions in V_{oc} and J_{sc}, but also a large drop in *FF* caused by higher series resistance (R_S) and lower shunt resistance (R_{SH}). The increase in R_S from 3.2 Ω cm^2 to 3.9 Ω cm^2 (Table 3) can be correlated with an increase in the thickness of the large-grained CZTSSe layer (Fig. 1). Compared with the clean surface and smooth grains of other samples, small particles (for example found inside the white dashed circle in Fig.4(a)) are dispersed on the absorber after a relatively long selenization time and are likely to account for the degeneration in device

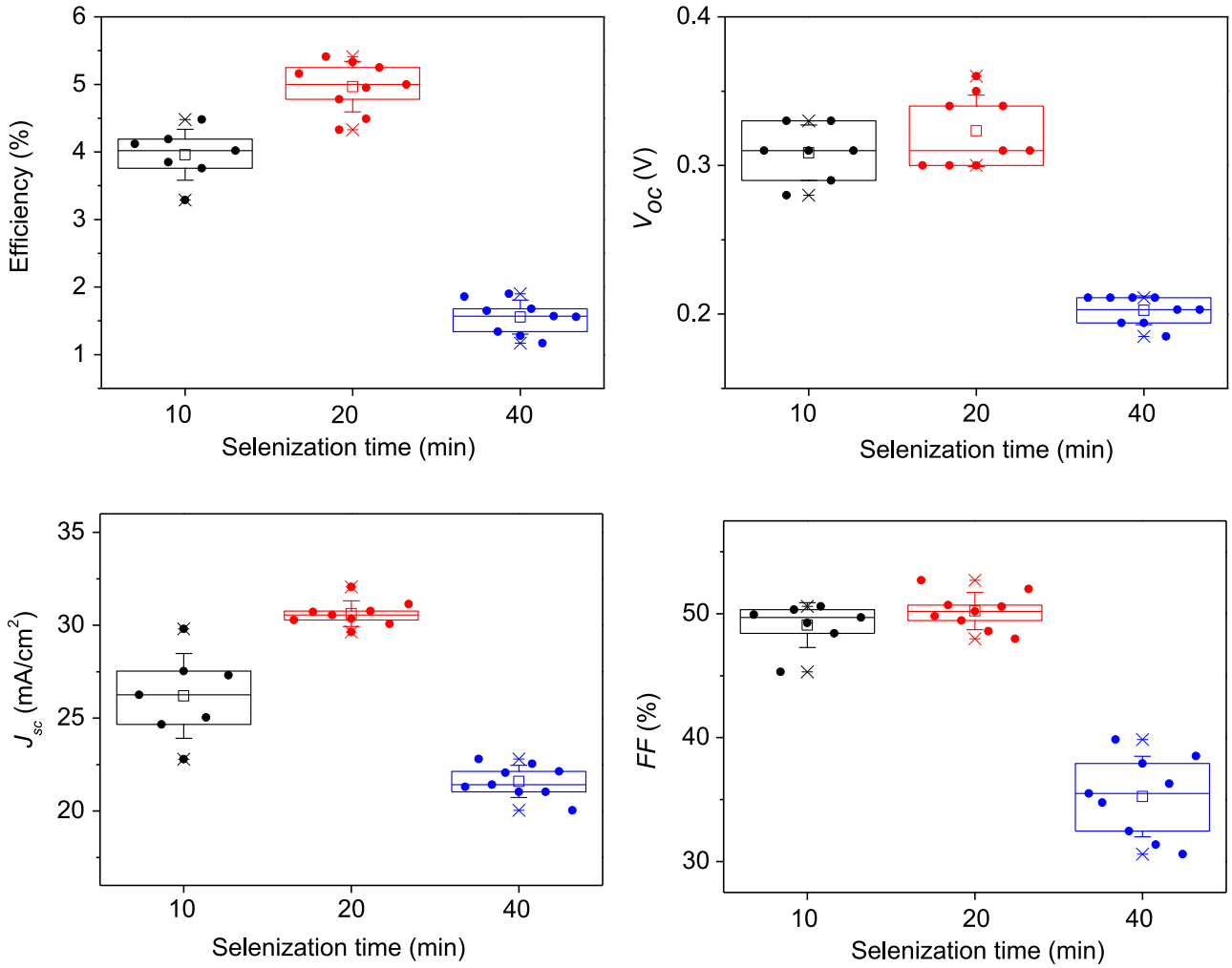

Fig. 8. Performance distributions of solar cells fabricated using CZTSSe thin films annealed different times. □ is the average value and × is the minimum and maximum position. The three horizontal lines of each box stand for the 25%, 50% and 75% of the reading distribution. The whisker range is determined by the standard deviation of the nine devices per substrate.

Table 4
Device parameters for the solar cells with *J–V* curves shown in Fig. 7(b).

Device (°C)	η (%)	V_{oc} (V)	J_{sc} (mA/cm^2)	*FF* (%)	R_S (Ω cm^2)	R_{SH} (Ω cm^2)
450	0.82	0.21	14.6	26.9	13.9	17
500	5.41	0.36	29.6	50.7	3.1	77
550	1.32	0.21	19.8	31.8	5.5	14
600	0.22	0.05	1.5	28.5	137.6	156

performance. The particles were too small to resolve any compositional information by EDS however, they could be Se condensed on the thin film surface. This is currently not well understood and requires further investigation. The reason for this is currently not well understood and needs further investigation. Inspection of the device parameter distributions summarized in Fig. 8 shows that the relatively low efficiency of the 10 min annealed sample mainly arises from inferior J_{sc} compared with the 20 min annealed sample. Longer annealing time causes more selenium incorporation into the lattice and thicker, large-grained layers are developed, which account for more efficient absorption of the incident light.

The influence of the selenization temperature on the device performance was also considered. *J–V* curves of the best device at each selenization temperature are shown in Fig. 7(b) with the device parameters extracted from the *J–V* curves summarized in Table 4. The variations in device performance for all nine devices on each substrate are also shown in Fig. 9.

The selenization temperature plays an important role in determining the device performances due to its significant influence on the absorber morphology. For CZTS thin films selenized at low temperature, small and loosely packed grains are obtained as shown in Fig. 5(a). These thin films only yield inferior devices with poor device parameters which degrade the device efficiency to only ~1.0%. When the treatment temperature increases to 500 °C, larger grains are obtained. Perhaps more importantly, the grains become densely packed and yield smooth and crack free thin films (Fig. 5(b)). From the cross-sectional views shown in Fig. 5(e–h), thicker large-grained layers and thinner fine-grained layers are developed at higher temperature. This is thought to improve the device performance by enhancing absorption of low energy photons and reducing parasitic resistance [11]. Using these thin films, devices with efficiencies of up to 5.41% are achieved. However, for samples annealed at higher temperatures such as 550 °C and 600 °C, the detrimental effects of holes on the surface of the absorber (as indicated by the arrows in Fig. 5(c–d)) can be observed as the device efficiency is reduced. Therefore, it is crucial to optimize the selenization conditions to find the optimum balance between grain growth and thin film stability. Furthermore, compared with 550 °C the device with absorber annealed at, 600 °C exhibits even worse performance with almost no diode

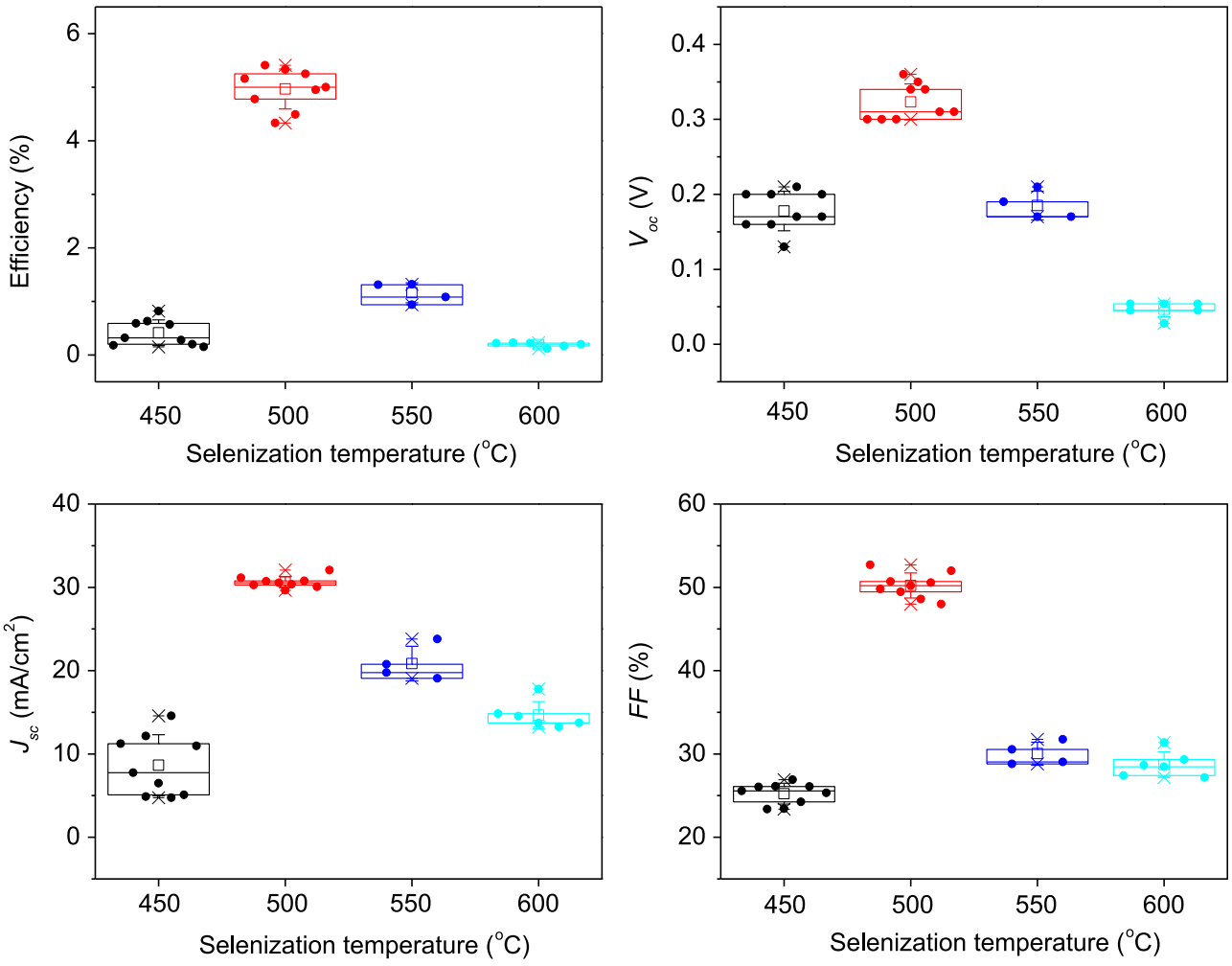

Fig. 9. Performance distribution of solar cells fabricated using CZTSSe thin films annealed at different temperatures. □ is the average value and × is the minimum and maximum position. The three horizontal lines of each box stand for the 25%, 50% and 75% of the reading distribution. The whisker range is determined by the standard deviation of the nine readings.

characteristic. A possible reason is a thicker $Mo(S,Se)_2$ interfacial layer is formed (as shown in Fig.5(h)) and although thin $Mo(S,Se)_2$ interfacial layers are widely found in high efficiency solar cells [8,14], too thick a layer will limit the device performance as a consequence of high resistivity and poor adhesion [20,21].

Although not the focus of this work, it is also possible to comment on the impact of the small grain layer. In CIGS technology where a two-step process is employed, a bilayer structure is indicative of unreacted material and undesirable for device performance. However this is not the case for CZTSSe fabricated from nanoparticles as the small grained layer contains the desired kesterite phase and has been shown by Wu et al. not to degrade performance [22]. Indeed the small grained layer is thought to improve the Ohmic back contact a known deficiency in CZTSSe solar cells. In addition our work confirms that a reduction in the thickness of the thin grain layer is not indicative of higher cell efficiency and that optimization of the large grain layer and $Mo(S,Se)_2$/Mo interface is of higher priority for improving the efficiency of CZTSSe. This aspect of CZTSSe thin film solar cells made from nanoparticle inks lacks detailed understanding and merits further investigation.

4. Conclusions

High quality CZTSSe photovoltaic absorber layers were fabricated by selenizing the as-deposited thin film made from CZTS nanoparticle inks. Selenization time and temperature are found to significantly affect the morphology and composition of the thin film. Longer time and higher temperature result in larger CZTSSe grains and more selenium being incorporated into the lattice. The reaction of the CZTS selenization process is controlled by cation re-ordering and grain boundary migration (Avrami's model) rather than selenium incorporation (parabolic model). CZTS is widely recognised to be an inherently disordered material and this work demonstrates that cation reordering plays a significant role in the selenization process. The CZTSSe grain growth follows normal grain growth behavior. It is found that an energy of 85.38 kJ/mol is needed to activate the CZTSSe boundary migration to consume the small grains and grow larger grains. Furthermore, relatively moderate selenization conditions of 500 °C for 20 min yields a peak device efficiency of 5.4%. The device performance is highly sensitive to the selenization conditions, indicating that it is

essential to find the correct balance between grain growth and thin film quality.

Acknowledgments

NB and GZ gratefully acknowledge funding from the Royal Society (Research grant R120090).

References

[1] H. Zhou, W.C. Hsu, H.S. Duan, B. Bob, W. Yang, T.B. Song, C.J. Hsu, Y. Yang, CZTS nanocrystals: a promising approach for next generation thin film photovoltaics, Energy Environ. Sci. 6 (2013) 2822–2838.
[2] I. Repins, C. Beall, N. Vora, C. DeHart, D. Kuciauskas, P. Dippo, B. To, J. Mann, W.C. Hsu, A. Goodrich, R. Noufi, Co-evaporated $Cu_2ZnSnSe_4$ films and devices, Sol. Energy Mater. Sol. Cells 101 (2012) 154–159.
[3] B. Shin, O. Gunawan, Y. Zhu, N.A. Bojarczuk, S.J. Chey, S. Guha, Thin film solar cell with 8.4% power conversion efficiency using an earth-abundant Cu_2ZnSnS_4 absorber, Prog. Photovolt. Res. Appl. 21 (2013) 72–76.
[4] W. Yang, H.S. Duan, B. Bob, H. Zhou, B. Lei, C.H. Chung, S.H. Li, W.W. Hou, Y. Yang, Novel solution processing of high-efficiency earth-abundant $Cu_2ZnSn(S,Se)_4$ solar cells, Adv. Mater. 24 (2012) 6323–6329.
[5] M.T. Winkler, W. Wang, O. Gunawan, H.J. Hovel, T.K. Todorov, D.B. Mitzi, Optical designs that improve the efficiency of $Cu_2ZnSn(S,Se)_4$ solar cells, Energy Environ. Sci. 7 (2014) 1029–1036.
[6] G. Zoppi, I. Forbes, R.W. Miles, P.J. Dale, J.J. Scragg, L.M. Peter, $Cu_2ZnSnSe_4$ thin film solar cells produced by selenisation of magnetron sputtered precursors, Prog. Photovolt. Res. Appl. 17 (2009) 315–319.
[7] W. Wang, M.T. Winkler, O. Gunawan, T. Gokmen, T.K. Todorov, Y. Zhu, D.B. Mitzi, Device characteristics of CZTSSe thin-film solar cells with 12.6% efficiency, Adv. Energy Mater. 4 (2014) 1301465.
[8] C.K. Miskin, W.C. Yang, C.J. Hages, N.J. Carter, C.S. Joglekar, E.A. Stach, R. Agrawal, 9.0% efficient $Cu_2ZnSn(S,Se)_4$ solar cells from selenized nanoparticle inks, Prog. Photovolt. Res. Appl. 23 (2015) 654–659.
[9] Y. Qu, G. Zoppi, R.W. Miles, N.S. Beattie, Influence of reaction conditions on the properties of solution-processed Cu_2ZnSnS_4 nanocrystals, Mater. Res. Express 1 (2014) 045040.
[10] Y. Qu, G. Zoppi, N.S. Beattie, The role of nanoparticle inks in determining the performance of $Cu_2ZnSn(S,Se)_4$ thin film solar cells, Prog. Photovolt. Res. Appl. (2015), Submitted for publication.
[11] J. van Embden, A.S.R. Chesman, E. Della Gaspera, N.W. Duffy, S.E. Watkins, J.J. Jasieniak, $Cu_2ZnSnS_{4x}Se_{4(1-x)}$ solar cells from polar nanocrystal inks, J. Am. Chem. Soc. 136 (2014) 5237–5240.
[12] J. Zhong, Z. Xia, C. Zhang, B. Li, X. Liu, Y.B. Cheng, J. Tang, One-pot synthesis of self-stabilized aqueous nanoinks for $Cu_2ZnSn(S,Se)_4$ solar cells, Chem. Mater. 26 (2014) 3573–3578.
[13] J.J. Scragg, Studies of Cu_2ZnSnS_4 Films Prepared by Sulfurisation of Electrodeposited Precursors, University of Bath, Bath, UK, 2010.
[14] Y. Cao, M.S. Denny, J.V. Caspar, W.E. Farneth, Q. Guo, A.S. Ionkin, L.K. Johnson, M. Lu, I. Malajovich, D. Radu, H.D. Rosenfeld, K.R. Choudhury, W. Wu, High-efficiency solution-processed $Cu_2ZnSn(S,Se)_4$ thin-film solar cells prepared from binary and ternary nanoparticles, J. Am. Chem .Soc. 134 (2012) 15644–15647.
[15] W.K. Kim, S. Kim, E.A. Payzant, S.A. Speakman, S. Yoon, R.M. Kaczynski, R.D. Acher, T.J. Anderson, O.D. Crisalle, S.S. Li, V. Craciun, Reaction kinetics of α-$CuInSe_2$ formation from an In_2Se_3/CuSe bilayer precursor film, J. Phys. Chem. Solids 66 (2005) 1915–1919.
[16] W.K. Kim, E.A. Payzant, S. Yoon, T.J. Anderson, In situ investigation on selenization kinetics of Cu–In precursor using time-resolved, high temperature X-ray diffraction, J. Cryst. Growth 294 (2006) 231–235.
[17] C. Wagner, The evaluation of data obtained with diffusion couples of binary single-phase and multiphase systems, Acta Mater. 17 (1969) 99–107.
[18] R. Mainz, A. Weber, H. Rodriguez-Alvarez, S. Levcenko, M. Klaus, P. Pistor, R. Klenk, H.W. Schock, Time-resolved investigation of Cu(In,Ga)Se_2 growth and Ga gradient formation during fast selenisation of metallic precursors, Prog. Photovolt. Res. Appl. 23 (2014) 1131–1143, http://dx.doi.org/10.1002/pip2531.
[19] C.V. Thompson, Grain growth in thin films, Annu. Rev. Mater. Sci. 20 (1990) 245–268.
[20] B. Shin, Y. Zhu, N.A. Bojarczuk, S. Jay Chey, S. Guha, Control of an interfacial $MoSe_2$ layer in $Cu_2ZnSnSe_4$ thin film solar cells: 8.9% power conversion efficiency with a TiN diffusion barrier, Appl. Phys. Lett. 101 (2012) 053903.
[21] X. Zhu, Z. Zhou, Y. Wang, L. Zhang, A. Li, F. Huang, Determining factor of $MoSe_2$ formation in Cu(In,Ga)Se_2 solar cells, Sol. Energy Mater. Sol. Cells 101 (2012) 57–61.
[22] W. Wu, Y. Cao, J.V. Caspar, Q. Guo, L.K. Johnson, I. Malajovich, H.D. Rosenfeld, K.R. Choudhury, Studies of the fine-grain sub-layer in the printed CZTSSe photovoltaic devices, J. Mater. Chem. C 2 (2014) 3777–3781.